Cell Stem Cell
Article

A Human iPSC Model of Hutchinson Gilford Progeria Reveals Vascular Smooth Muscle and Mesenchymal Stem Cell Defects

Jinqiu Zhang,[1] Qizhou Lian,[3,4] Guili Zhu,[1] Fan Zhou,[1] Lin Sui,[1] Cindy Tan,[1] Rafidah Abdul Mutalif,[2] Raju Navasankari,[2] Yuelin Zhang,[3] Hung-Fat Tse,[3] Colin L. Stewart,[2,*] and Alan Colman[1,*]
[1]Stem Cell Disease Models
[2]Developmental and Regenerative Biology
A*STAR Institute of Medical Biology, Singapore 138648, Singapore
[3]Cardiology Division, Department of Medicine
[4]Eye Institute, Li Ka Shing Faculty of Medicine
University of Hong Kong, Pokfulam, Hong Kong, China
*Correspondence: colin.stewart@imb.a-star.edu.sg (C.L.S.), alan.colman@imb.a-star.edu.sg (A.C.)
DOI 10.1016/j.stem.2010.12.002

SUMMARY

The segmental premature aging disease Hutchinson-Gilford Progeria syndrome (HGPS) is caused by a truncated and farnesylated form of Lamin A called progerin. HGPS affects mesenchymal lineages, including the skeletal system, dermis, and vascular smooth muscle (VSMC). To understand the underlying molecular pathology of HGPS, we derived induced pluripotent stem cells (iPSCs) from HGPS dermal fibroblasts. The iPSCs were differentiated into neural progenitors, endothelial cells, fibroblasts, VSMCs, and mesenchymal stem cells (MSCs). Progerin levels were highest in MSCs, VSMCs, and fibroblasts, in that order, with these lineages displaying increased DNA damage, nuclear abnormalities, and HGPS-VSMC accumulating numerous calponin-staining inclusion bodies. Both HGPS-MSC and -VSMC viability was compromised by stress and hypoxia in vitro and in vivo (MSC). Because MSCs reside in low oxygen niches in vivo, we propose that, in HGPS, this causes additional depletion of the MSC pool responsible for replacing differentiated cells lost to progerin toxicity.

INTRODUCTION

Hutchinson-Gilford Progeria syndrome (HGPS) is a rare congenital disease that may cause some aspects of premature aging in children (Hennekam, 2006). Afflicted individuals generally die in their early teens due to myocardial infarction or stroke, but it is the wizened facial features and wasted bodies that have made this harrowing condition familiar to the population at large. The disease progression displays many symptoms of normal aging, such as severe growth retardation, alopecia, loss of subcutaneous fat, and progressive atherosclerosis, although other symptoms associated with aging such as neural degeneration, diabetes, malignancies, and cataracts are absent (Ackerman and Gilbert-Barness, 2002; Gordon et al., 2007; Merideth et al., 2008). This disease, which seems to affect mainly mesenchymal lineages, is caused by an autosomal dominant mutation in the *LMNA* gene (De Sandre-Giovannoli et al., 2003; Burke and Stewart, 2006; Capell and Collins, 2006). The most common (in 80%–90% of cases) mutation is a C-T transition at position 1824 in exon 11 that creates an efficient alternative splice donor site. This leads to the production of a truncated lamin A protein (progerin) with an internal deletion of 50 amino acids in the C-terminal globular domain. As a result of this mutation, progerin, but not mature lamin A, retains a C-terminal farnesyl tail that is normally only transiently present in the Lamin A precursor. Farnesyl retention is widely thought to underlie the intracellular disruption associated with progerin, although the exact roles of the farnesyl group and the deletion in the etiology of the disease are controversial (Yang et al., 2008).

The cell type-specific pathologies in HGPS have been attributed to a variety of causes, including progerin-mediated stem cell pool exhaustion (Halaschek-Wiener and Brooks-Wilson, 2007), mesenchymal lineage differentiation defects (Scaffidi and Misteli, 2008), a diminished DNA-damage-repair response (Musich and Zou, 2009), and nuclear fragility in mechanically stressed cells such as cardiomyocytes (Verstraeten et al., 2008). Interestingly, the same aberrant splicing event may also occur at much lower levels in normal cells (Scaffidi and Misteli, 2006). Although low progerin RNA levels may not increase with age, several reports have suggested that progerin protein levels do increase, (McClintock et al., 2007; Scaffidi and Misteli, 2006), possibly reflecting a low turnover of the protein or an age-related inability to remove cells with high progerin loads. This has led to speculation that studies on progeria may provide insight into the normal human aging process.

Due to the rarity and juvenile mortality of this disease, biopsy and autopsy analysis has been limited, although pronounced vascular smooth muscle loss and artherosclerosis appear to be critical factors contributing to the death of patients (Stehbens et al., 2001; Olive et al., 2010). Much of the information relating to the pathophysiology of HGPS has come from studies on patient-derived skin fibroblasts, wild-type and mutant lamin A overexpression in established cell lines (Cao et al., 2007; Goldman et al., 2004), and the development of various mouse models in

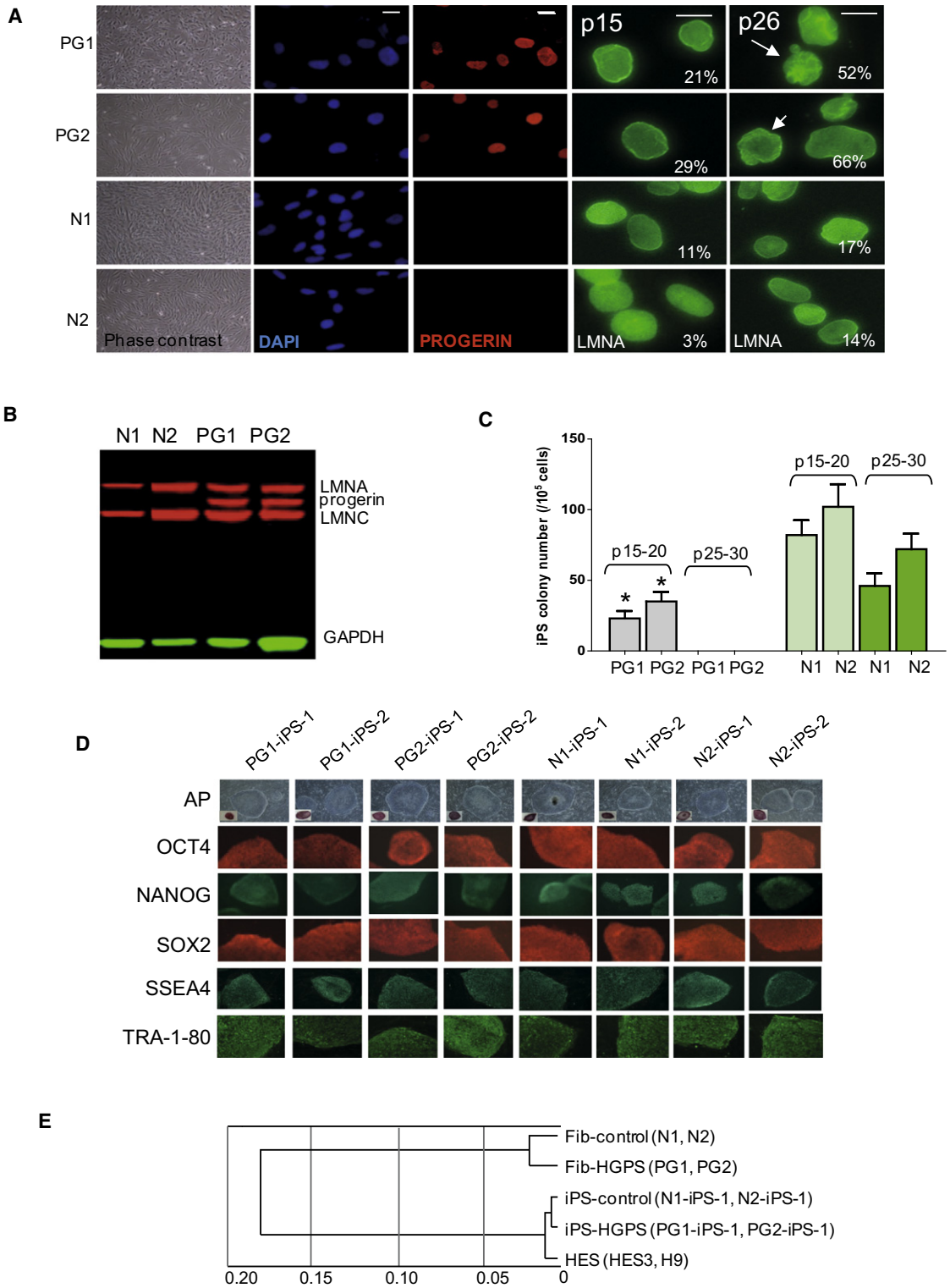

Figure 1. Generation of Patient-Specific iPSCs

(A) HGPS patient fibroblasts AG11498 (PG1) and AG06297 (PG2) were obtained from the Coriell Institute, and two unaffected HGPS parental fibrolast lines, AG03512 (N1) and AG06299 (N2), were used as controls. Immunofluorescence microscopy of fibroblast cells using an antibody specifically recognizing mutant LMNA (progerin) shows specific expression of progerin in HGPS patient fibroblasts, but not controls. Immunostaining with JOL2 antibody recognizing human LMNA/C (right panels) shows increasing nuclear deformation (arrows) in HGPS fibroblasts undergoing extended passaging from p15 to p26. The percentage of cells showing aberrant nuclei is indicated for respective passages. Scale bar, 20 μm.

(B) Progerin expression in donor fibroblasts. Western blot analysis of fibroblast lysates using the JOL2 antibody recognizes both human LMNA and -C.

which the lamin A gene is deleted, mutated, and/or overexpressed (Mounkes et al., 2003; Yang et al., 2005; Varga et al., 2006; Sagelius et al., 2008; Hernandez et al., 2010). The use of mouse models has been particularly informative; however, no one mouse model recapitulates all the symptoms seen in the human disease.

Recently, a number of human disease models have been established by the transcription-factor-mediated reprogramming of somatic cells taken from patients with Lou Gehrig's disease (Dimos et al., 2008), spinal muscular atrophy (Ebert et al., 2009), familial dysautonomia (Lee et al., 2009), and dyskeratosis congenita (Agarwal et al., 2010). In all cases, the reprogrammed cells (induced pluripotent stem cells [iPSCs]) were used to derive cell types that, in vivo, display a distinctive disease phenotype. The underlying hope behind these studies is that a disease pathology will emerge in a relatively short time (compared to disease progression in vivo) and generate insight into early disease pathophysiology, as well as providing cell types for drug screening and discovery.

Here, we describe an iPSC model of HGPS. iPSC lines were made from patient-derived fibroblasts and differentiated into mesenchymal and nonmesenchymal lineages to analyze the impact of progerin on the functional properties of the different cell types. We find that progerin levels are highest in mesenchymal stem cells, VSMCs, and fibroblasts, and lowest in the neural progenitors. Progerin expressing VSMCs and MSCs, but not controls, are sensitive to hypoxia, and HGPS-MSCs fail to mediate circulatory restoration in a murine hind limb recovery model. We speculate that one significant cause of progeria pathology is a shortage of MSCs needed for tissue replacement, and this shortage is exacerbated by a loss of specific differentiated types due to progerin. Our experiments support the hypothesis that the MSC pool becomes exhausted due to replicative overload in HGPS patients (Halaschek-Wiener and Brooks-Wilson, 2007), which is compounded by a parallel depletion due to progerin-induced sensitivity of the stem cells to their niche conditions.

RESULTS

Generation of HGPS-iPSCs

Skin-derived fibroblast cultures from two HGPS patients (AG11498 [PG1], AG06297 [PG2]) and two HGPS parents (AG03512 [N1], AG06299 [N2]) were obtained from the Coriell Institute. Both patient genomes contain the typical C-T mutation of *LMNA* gene at position 1824 of exon 11. The mutant protein, progerin, was detected exclusively in HGPS fibroblasts by western analysis and immunofluorescence using a progerin-specific antibody (Figure 1). Nuclear membrane deformation "blebbing" was seen in approximately 20%–30% HGPS fibroblasts at p15-20, in contrast to 3%–11% in normal fibroblast cells at similar passage. This increased to 60%–70% in HGPS fibroblasts by p25-30, with more modest increases seen in the control fibroblasts. PG1, PG2, and N2 fibroblasts displayed normal karyotypes. However, in N1 fibroblasts, 55% of cells had an abnormal karyotype with trisomy 7. We reprogrammed the four fibroblast lines by retrovirus infection of cells at p15-20 using the "Yamanaka" factor cocktail: OCT4, SOX2, KLF4, and C-MYC. Infected fibroblasts were cultured on a murine feeder layer with 0.5 mM valproic acid in human ESC medium. iPSC colonies were observed at 2 to 3 weeks and picked between 3 to 4 weeks. Though the efficiency of reprogramming of HGPS fibroblasts was 4-fold lower than parental control fibroblasts (Figure 1C), all the colonies picked were expanded and displayed morphologies indistinguishable from human ESCs (Figure 1D): no colonies were obtained from the two HGPS fibroblast cultures at late passage (p26). We attribute this failure to the onset of senescence observed in these cultures beginning at p22 since efficient iPSC generation is associated with a cell's proliferative potential (Hanna et al., 2009). Five to ten colonies were picked to represent each patient or control, and for the N1-iPSC, about 50% of the colonies displayed a normal karyotype.

Characterization of iPSCs

Exogenous expression of the four reprogramming factors was screened for by RT-PCR in all the iPSC clones. No transgenic transcripts were found in any clone (Figure S1A available online). Two clones from each patient or control (given the suffix iPSC-1 or iPSC-2) each with a normal karyotype (Figure S1B) were selected for further characterization. DNA sequencing revealed HGPS-iPSC but no control clones had the C-T mutation of the *LMNA* gene (Figure S1C). All clones express the pluripotent markers OCT4, SOX2, NANOG, SSEA4, and TRA1-80, as determined by immunocytochemistry (Figure 1D). In addition, all iPSC lines showed reactivation of three endogenous pluripotency-related genes with similar level of expression as seen in hESCs (Figure S2A). As expected for hiPSCs, the *OCT4* promoter region in all iPSCs (and hESC3) was hypomethylated in contrast to its hypermethylated state in the parental fibroblasts (Figure S2B). To test the pluripotency of iPSCs, teratoma assays were performed in SCID mice. All the clones developed teratomas comprised of tissues from all three germ layers (Figure S2C). The transcriptomes of two independently derived sister clones from each hiPSC genotype were compared to that in two different hESC lines (hESC3 and H9) by microarray analysis on 24,000 gene Illumina chips. Clustering analysis revealed a high degree of similarity ($r = 0.99$) between the reprogrammed HGPS-iPSCs (PG1-iPSCs, PG2-iPSCs) and parental control

(C) Reduced reprogramming efficiency of HGPS fibroblasts. Efficiencies were calculated as number of alkaline phosphatase positive colonies at day 21 after transduction of 10^5 HGPS (PG1, PG2) or control (N1, N2) fibroblasts by retroviruses carrying OSKM. *$p < 0.01$, $n = 3$. No iPS colonies were obtained for late passage (p25–p30) HGPS fibroblasts.

(D) Immunohistology of iPSC clones. Phase contrast (row 1) with alkaline phosphatase (AP) staining (inset) and immunofluorescence staining of iPSCs (remaining rows) for the following pluripotent markers: OCT4, SOX2, NANOG, SSEA-4, and Tra-1-81. Two iPS clones were analyzed for each line.

(E) Cluster analysis of microarray data from HGPS fibroblast (PG1, PG2), control fibroblast (N1, N2), HGPS-iPSC (PG1-iPS-1, PG2-iPS-1), control iPSC (N1-iPS-1, N2-iPS-1) and human ESC (HES3, H9) RNA. The Pearson correlation coefficient (PCC) was calculated for each pair of samples (see Table S1) using the relative expression level of all transcripts. Hierarchical cluster analysis was carried out with PCC as the distance measurement using Illumina GenomeStudio software. See also Figures S1 and S2 for characterization of iPSCs.

iPSC (N1-iPSCs, N2-iPSCs) that clustered with the hESC group (r = 0.99). The three groups were distant from the HGPS and control fibroblasts (r = 0.82) (Figure 1E, Table S1). The above data indicate that, despite the presence of progerin in the nucleus, somatic cells from HGPS patients can be reprogrammed into iPSCs with characteristics that are highly similar to embryo-derived human ESCs.

LaminA/C and Progerin Expression Are Silenced by Reprograming

Lamins A and C are transcribed from the same promoter and share the first 566 amino acids. Undifferentiated mESCs and hESCs do not express *LMNA* transcripts (Constantinescu et al., 2006). Immunofluorescent analysis of the iPSC colonies revealed that LMNA proteins were expressed in differentiated cells at the edge of the colony, whereas the bulk of the colony stained for the pluripotent marker SOX2 (Figure 2A). No specific staining for progerin was detected in any region. Quantitative RT-PCR analysis confirmed the presence of *LMNA* transcripts but showed progerin transcripts present at lower levels. Colony dissection indicated that the majority of these transcripts were at the rim of the colonies (Figure 2B). In addition, RNA levels of *LMNA* and progerin expression in intact HGPS-iPSC colonies were less than 10% of those present in fibroblasts (Figure 3A). These data demonstrate that *LMNA* expression in patient and control fibroblasts was suppressed by reprogramming.

Differentiation of iPSCs

Clinical and autopsy data indicate that in HGPS, the main lineages affected are mesenchymal in origin with neural lineages seemingly unaffected (McClintock et al., 2006; Merideth et al., 2008). Since tissue samples from HGPS patients are extremely rare, we used existing or modified protocols to derive MSC, neural, and other candidate lineages for further examination.

LMNA and Progerin Are Re-expressed during iPSC Differentiation

Differentiation of the HGPS-iPSC clones always resulted in expression of lamins A, C, and progerin. We quantified lamin A and C expression by both western and real-time RT-PCR analysis (Figures 3A and 3B). Progerin levels were highest in iPSC-derived mesenchymal stem cells (MSCs), followed by vascular smooth muscle cells (VSMCs), fibroblast, and endothelial cells, in that order. Neural progenitors consistently showed the lowest levels. Interestingly, we observed a 3- to 5-fold increase in progerin levels over prolonged culture for iPSC-MSCs (Figure 3C), whereas in only one of the two HGPS-iPSC fibroblast lines was an increase noted (data not shown). A similar inconsistency in progerin accumulation, with passage number in patient fibroblasts, was previously reported (Goldman et al., 2004; Verstraeten et al., 2008). Overall, our observations are consistent with skin biopsy data in finding significant presence of progerin in endothelial and fibroblast lineages.

Impact of the HGPS Mutation on Fibroblast, Neural Progenitor, Endothelial, and MSC Functions under Normal Culture Conditions

Extended culture of HGPS and control fibroblasts revealed an accumulation of abnormal nuclear morphologies (Bridger and Kill, 2004). We obtained fibroblasts by FACS sorting of Thy1$^+$ cells formed during differentiation of the iPSC lines. The purified cells expressed prolyl 4-hydroxylase and displayed a similar surface marker profile to parental fibroblasts—high in CD29, CD44, and CD90 (Thy1) and low in CD106 (Figure 4A and Figure S3A). As with the HGPS-iPSC fibroblasts, we found

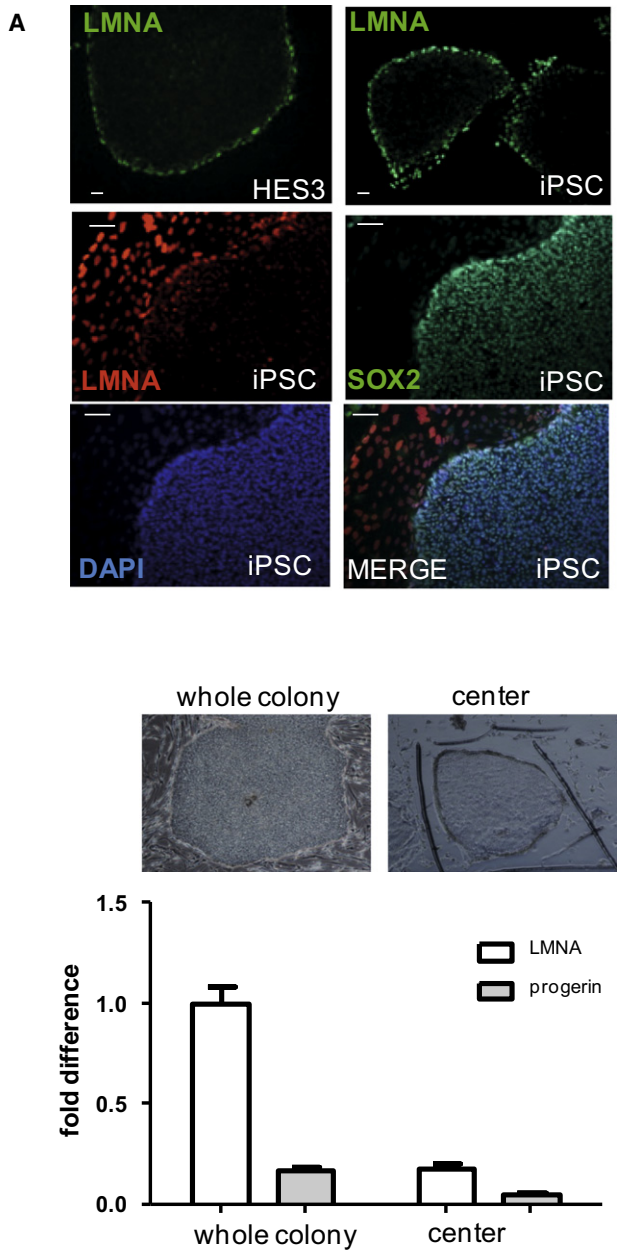

Figure 2. Expression of LMNA and Progerin Is Suppressed in iPSCs

(A) Immunofluorescence staining of LMNA/C on human ESC line HES3 and HGPS iPSCs (PG1) with JOL2 antibody shows LMNA/C expression in differentiated cells lining the edge of colonies. Costaining of LMNA/C with SOX2 shows suppressed expression of LMNA/C in pluripotent iPSCs. Scale bar, 50 μm.

(B) qPCR of *LMNA* and *progerin* expression in HGPS-iPSCs after colony dissection. Most expression was seen at the colony edges where differentiation was occurring.

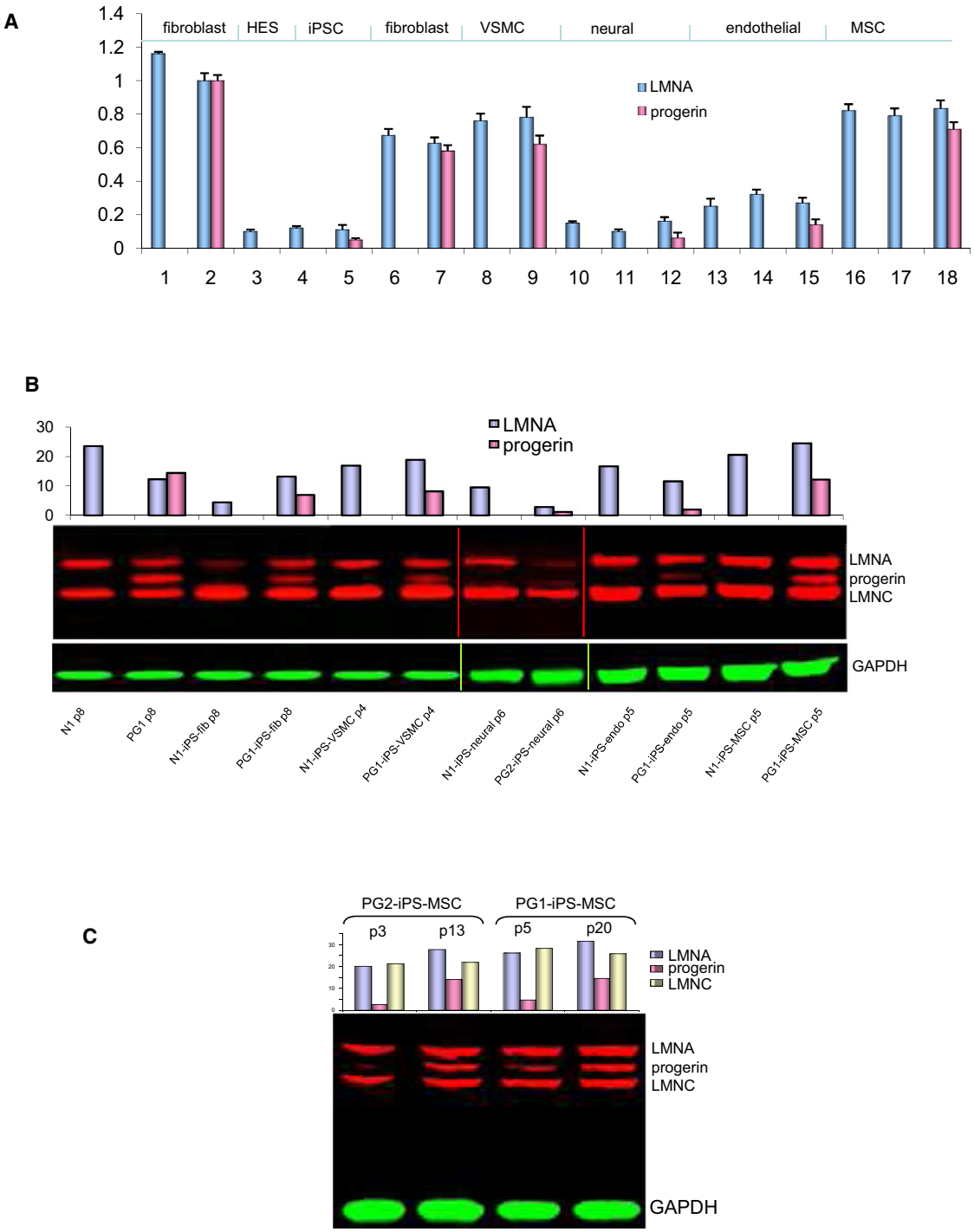

Figure 3. *Lamin A/C* Expression in iPSC-Derived Fibroblasts, Endothelial Cells, Neural Progenitor Cells, VSMCs, and MSCs

(A) Relative *Lamin A* and *progerin* expression in iPSC differentiated samples by RT-PCR using Taqman probes. *LMNA* and *progerin* expression were each set as 100% for PG1 samples. Commercially available cell lines were used as references for each lineage: (1) N1 fibroblast p10, (2) PG1 fibroblast p10, (3) HESC3 p83, (4) N1-iPSC-1 p11, (5) PG1-iPSC-1 p13, (6) N1-iPSC-fibroblast p10, (7) PG1-iPSC-fibroblast p10, (8) N1-iPSC-VSMC p3, (9) PG1-iPSC-VSMC p3, (10) ReNcell human fetal neural stem cell line, (11) N1-iPSC-neural p5, (12) PG1-iPSC-neural p5, (13) human umbilical vein endothelial cell line HUVEC p5, (14) N1-iPSC-endo p5, (15) PG1-iPSC-endo p6, (16) human adult bone-marrow MSC p5, (17) N1-iPSC-MSC p6, and (18) PG1-iPSC-MSC p6. Data were normalized to GAPDH expression. (B) Quantitative analysis of LMNA and progerin by western blot. Twenty micrograms of total protein extracts were loaded, and protein expression was quantitatively analyzed with the Odyssey infrared imaging system. Values represent relative densitometry normalized to GAPDH. The passage number of each sample is indicated. The picture is combination of three separate blots which contained N1 and PG1 fibroblast lysates in each blot as the internal control. (C) Accumulation of progerin in HGPS-iPSC-MSCs during extended passaging. Quantitative western blot shows progerin protein accumulation in two different patient-derived HGPS-iPSC-MSCs.

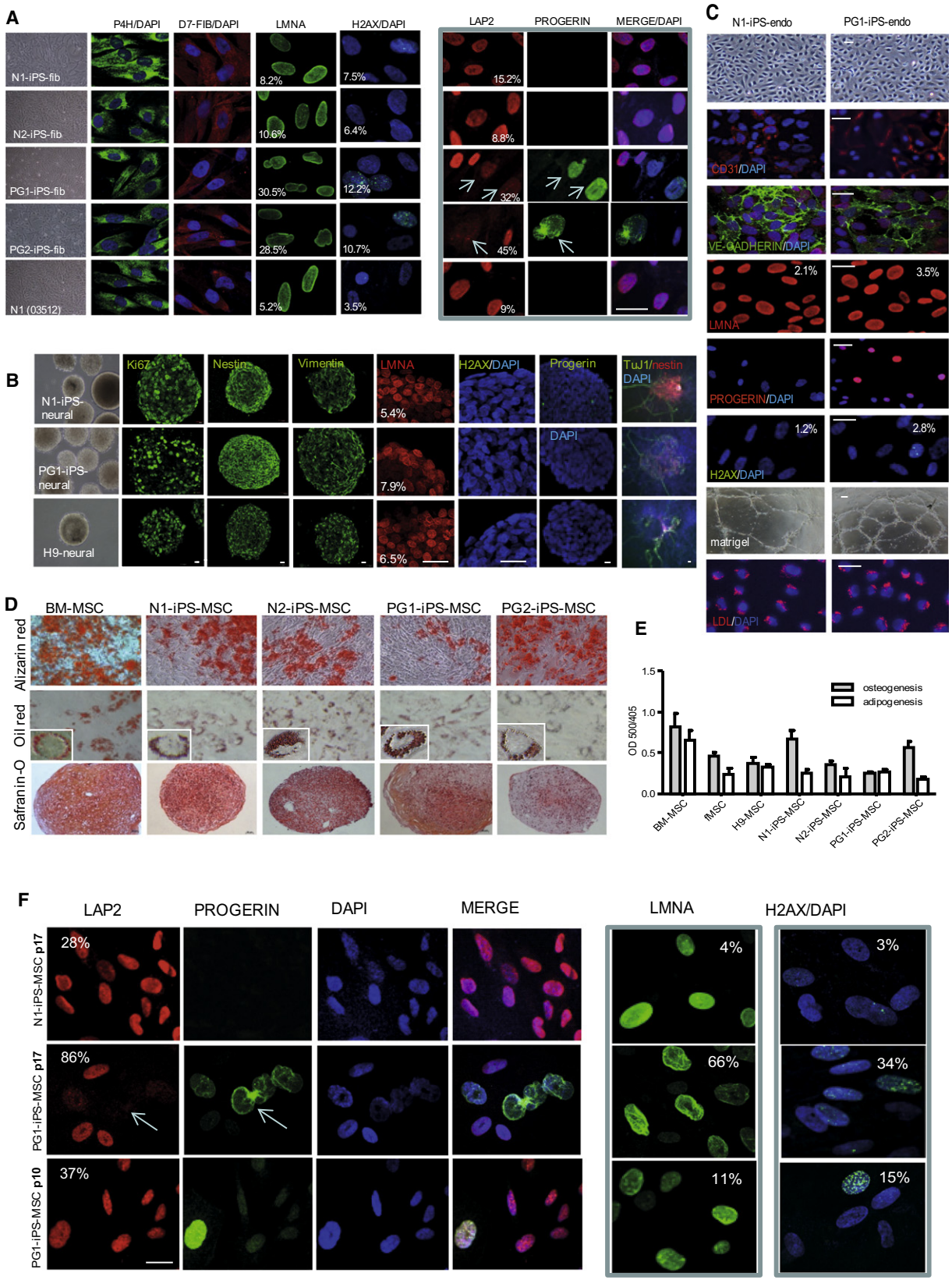
A
P4H/DAPI
D7-FIB/DAPI
LMNA
H2AX/DAPI
LAP2
PROGERIN
MERGE/DAPI
N1-iPS-fib
N2-iPS-fib
PG1-iPS-fib
PG2-iPS-fib
N1 (03512)
8.2%
7.5%
10.6%
6.4%
30.5%
12.2%
28.5%
10.7%
5.2%
3.5%
15.2%
8.8%
32%
45%
9%
B
Ki67
Nestin
Vimentin
LMNA
H2AX/DAPI
Progerin
TuJ1/nestin DAPI
N1-iPS-neural
PG1-iPS-neural
H9-neural
5.4%
7.9%
6.5%
DAPI
C
N1-iPS-endo
PG1-iPS-endo
CD31/DAPI
VE-CADHERIN/DAPI
2.1%
3.5%
LMNA
PROGERIN/DAPI
1.2%
2.8%
H2AX/DAPI
matrigel
LDL/DAPI
D
BM-MSC
N1-iPS-MSC
N2-iPS-MSC
PG1-iPS-MSC
PG2-iPS-MSC
Alizarin red
Oil red
Safranin-O
E
OD 500/405
1.5
1.0
0.5
0.0
osteogenesis
adipogenesis
BM-MSC
fMSC
H9-MSC
N1-iPS-MSC
N2-iPS-MSC
PG1-iPS-MSC
PG2-iPS-MSC
F
LAP2
PROGERIN
DAPI
MERGE
LMNA
H2AX/DAPI
N1-iPS-MSC p17
PG1-iPS-MSC p17
PG1-iPS-MSC p10
28%
86%
37%
4%
66%
11%
3%
34%
15%

increased nuclear dysmorphology, DNA damage (% nuclei with 3 or more foci staining for γ-H2AX), and mislocalization of the nuclear protein, LAP2, in progerin-expressing lines (Figure 4A). Progerin accumulation was heterogeneous in the HGPS populations, and loss of LAP2 from the nuclei was more apparent in nuclei displaying higher progerin levels and more pronounced dysmorphology (Figure 4A, arrows). These results are similar to those for HGPS patient fibroblasts after extended culture (Scaffidi and Misteli, 2006).

Neither increased DNA-damage foci nor nuclear dysmorphologies were observed in iPSC-derived neural progenitors and endothelial cells (Figures 4B and 4C). Neural progenitors were propagated by neurosphere culture and characterized by nestin, vimentin, and Ki67 staining (Figure 4B). Endothelial cultures were $CD31^{+ve}/CD43^{-ve}$, stained for VE-cadherin (Figure 4C) and were also positive for CD31, VE-cadherin, C-KIT, and KDR transcripts (Figure S3B). Neural progenitors made from different hESC or iPSC lines at passages 7–10 were differentiated mainly into Tuj-1^{+ve} neurons (Figure 4B), although some GFAP-staining glial cells were detected (data not shown). No differences were observed between HGPS and normal neurospheres in growth or neuronal differentiation. Both HGPS and control iPSC-derived endothelial cells formed lattice-like vessel structures on Matrigel (Figure 4C), a characteristic feature of endothelial cells. HGPS-iPSC endothelial cells also displayed a normal lipid uptake function (Figure 4C).

MSCs were prepared from iPSC-derived EBs and were characterized by FACS analysis as negative or low for the surface markers of CD24, CD31, and CD34 and positive for CD29, CD44, CD73, CD105, and CD166 (Figure S3C). Cluster analysis of microarray data indicated that the iPSC-MSCs were more closely related to hESC-derived and fetal bone marrow-derived MSCs than adult bone marrow MSCs (Figure S3D).

MSCs differentiate into osteogenic, chondrogenic, and adipogenic lineages in vitro when provided with appropriate growth conditions. All three lineages were formed from all the HGPS- and control-iPSC-MSC lines (Figures 4D and 4E). Under extended culture, the HGPS-MSCs showed considerable nuclear lobulation that correlated with increasing levels of progerin. The high percentage of nuclear malformation was accompanied by mislocalization of LAP2 (Figure 4F). A significant increase in nuclei-containing DNA damage foci was also observed in late passage HGPS-MSCs (Figure 4F).

VSMC were obtained from iPSC derived MSCs by treatment with a combination of SPC and TGFβ1 (Jeon et al., 2006). After 3 weeks of induction, 50%–60% cells showed specific VSMC marker expression of α-smooth muscle actin, calponin 1, and smooth muscle myosin heavy chain (Figure 5A) with the VSMC lineage marker transcripts being confirmed by RT-PCR (Figure 5B). The VSMCs displayed a characteristic spindle-like morphology and were induced to contract by carbachol administration (Figure 5C), supporting their VSMC identity. Like fibroblasts and MSCs, the HGPS-VSMCs displayed nuclear deformations, LAP2 mislocalization, and increased DNA damage on culture (Figure 5D). We also noticed that many, though not all, the calponin 1-staining HGPS-VSMC cells had vesicular-like calponin 1 inclusions (Figure 5A), which were absent in control and N-VSMCs. Although calponin decorates the filamentous actin cytoskeleton, we observed no costaining of actin with these bodies.

Patient iPSC-Derived VSMCs and MSCs Show Functional Defects under Stress

Of the five lineages we derived, two (HGPS-iPSC-derived VSMCs and MSCs) seem most adversely affected by progressive culture under normoxic conditions. This might reflect the higher levels of progerin these cell types appear to accumulate, although fibroblasts levels are only slightly lower (Figure 3B). We investigated whether other functional properties of these cells were impaired.

VSMCs were subjected to three different conditions of stress: hypoxia with substratum deprivation, hypoxia alone, and recurrent electrical stimulation. When HGPS-VSMCs were immersed under mineral oil for 4 to 5 hr (substratum deprivation/hypoxia), their survival was more than halved (Figure 6A). Hypoxia (2% O_2) for 3 days also increased senescence in HGPS-VSMCs, shown by β-galactosidase staining (5.1% to 38.5%, Figure 6B). To mimic the mechanical stresses endured by VSMCs in vivo

Figure 4. Characterization of iPSC-Derived Fibroblast-like Cells, Endothelial Cells, Neural Progenitor Cells, and MSCs

(A) Differentiation of iPSCs into fibroblast-like cells. Left panel: phase contrast pictures and immunofluorescence staining of iPSC derived fibroblasts using antibodies against P4H, fibroblasts (D7-FIB), LMNA and H2AX. Right panel, Progerin accumulation leads to aberrant expression of LAP2 in fibroblasts. Co-localization of LAP2 and progerin by immunostaining showed increased number of blebbed nuclei associated with mis-localization of LAP2 (arrows) in iPSC-fibroblast. The percentage of cells showing aberrant phenotypes is indicated. The parental fibroblast N1 (03512) was used as a control. Scale bar, 15 μm.

(B) Characterization of iPS-derived neural progenitor cells. Immunostaining showed that both HGPS and control iPSC-derived neurospheres expressed neural progenitor markers Ki67, nestin and vimentin and were able to differentiate into neurons with expression of βIII-tubulin (TuJ1) upon withdrawal of growth factors. Progerin and H2AX staining (green fluorescence) is rarely detected. The percentage of cells showing aberrant phenotypes is indicated. DAPI stains nuclei a blue color. Scale bar, 50 μm.

(C) Differentiation of iPSCs into endothelial cells. Phase contrast pictures showing the endothelial morphology and immunofluorescence staining with endothelial specific markers, CD31 and VE-Cadherin. The percentage of cells showing aberrant phenotypes and DNA damage is indicated. Lower panels show live imaging of Dil-AC-LDL uptake of iPSC-derived endothelial cells. Scale bar, 20 μm.

(D) Differentiation of MSCs into bone, cartilage, and adipocyte. Bone marrow MSCs, HGPS-iPSC-MSCs, and control-iPSC-MSCs were induced to undergo osteogenesis, adipogenesis, and chondrogenesis. Oil red, Safranin-O, and Alizarin red were used for staining of lipid oil droplet (adipocyte), proteoglycans and glycosaminoglycans (cartilage), and mineralization (bone), respectively.

(E) Semiquantitative analysis of adipogenesis and osteogenesis of MSCs. Oil red O was eluted with isopropanol and measured OD at λ500 nm. Alizarin red staining was semiquantitatively analyzed at 405 nm using a plate reader. Values represent mean ± SEM from three replicates.

(F) Progerin accumulation leads to aberrant expression of LAP2 in late passage MSCs. Colocalization of LAP2 and progerin by immunostaining showed increased number of blebbing nuclei associated with mislocalization of LAP2 in HGPS-MSCs from p10 to p17. Nuclear blebbing with strong expression of progerin (arrows) is associated with mislocalization of LAP2. The percentage of cells showing abnormal phenotypes is indicated. Scale bar, 15 μm.

See also Figure S3 and Tables S1–S3 for further characterization of iPSC-derived lineages.

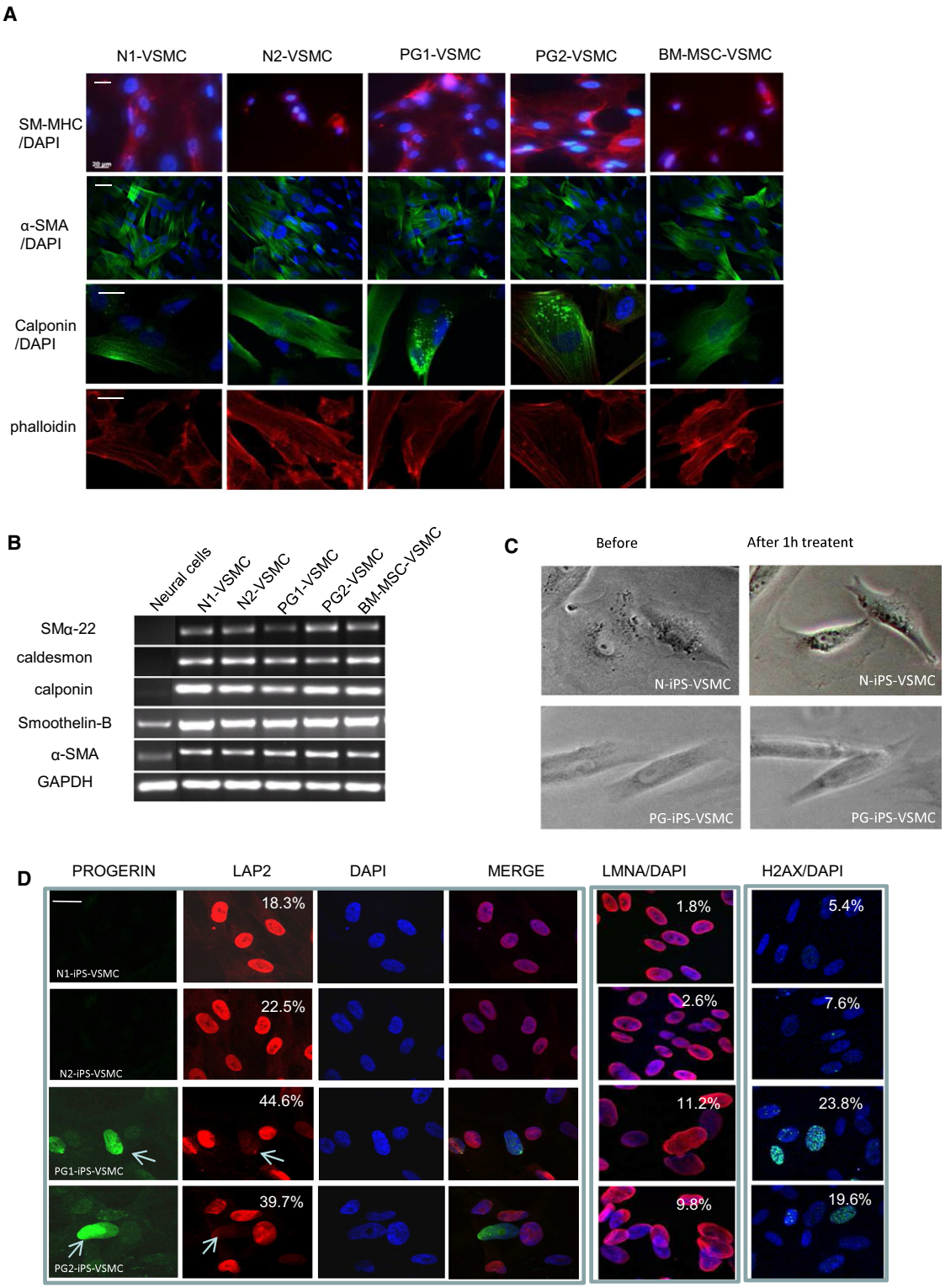

Figure 5. Characterization of iPSC-Derived Vascular Smooth Muscle Cells

(A) Immunostaining of vascular smooth muscle cells (VSMCs) showed expression of α-smooth muscle actin (α-SMA), calponin, and VSMC exclusive marker smooth muscle myosin heavy chain (SM-MHC). Lower panel shows colocalization of F-actin (phalloidin) with calponin. Scale bar, 15 μm.

(B) RT-PCR analysis of VSMC-specific contractile protein transcripts, α-SMA, calponin, smoothelin-B, *h*-caldesmon, and SMα-22. Neural cell line ReNcell was used as control.

(C) Induction of contraction by carbachol treatment. Phase contrast image shows contraction of VSMCs under carbachol (1×10^{-5}M) treatment for 1 hr (right panel).

due to pulsatile circulation, repeated contraction of VSMCs was chronically induced with electrical pulses (40V/cm, 1Hz) for 3 days. We observed an increase in nuclear dysmorphology and accelerated senescence in both HGPS-VSMC and N-VSMCs, although the effect was significantly greater with the HGPS-VSMCs (Figure 6C).

Although the exact roles of MSCs in vivo are unclear, human MSCs from bone marrow (Li et al., 2009) or from human embryonic stem cells (Lian et al., 2010) significantly improve vascular circulation after their transplantation into the ischemic hind limbs of immunocompromised mice. As a measure of their capacity to effect such improvement, we tested parental control (N-MSC)- and HGPS-iPSC-derived MSCs (HGPS-MSC) to protect against ischemia in this mouse model. Mouse limb ischemia was induced by ligation of the femoral artery and its branches in the left hind-limb of SCID mice. The MSCs were transplanted by intramuscular injection into the left hind-limb immediately after ligation. After 28 days of transplantation, the culture medium-injected group (vehicle group) displayed severe necrosis of the ischemic limbs leading to limb loss (87.5%; Figure 7A). In the 15 mice given an N-MSC injection, limb loss was only 20%. Most of the ischemic limbs were fully rescued (60%) or displayed moderate necrosis from knee to toe. However, in the 15 mice given HGPS-MSCs, rescue of ischemic limb occurred in only one mouse (6.7%). Most mice suffered limb loss (60%), which is significantly different from that seen with N-MSCs (Figure 7A). Histological analysis of the adductor muscle of the ''rescued'' limbs revealed extensive muscle degeneration and pronounced interstitial fibrosis in the HGPS–MSC group. The N-MSC mice, in contrast, exhibited significantly less fibrosis and more muscle regeneration (Figure S4).

The simplest explanation for limb salvage was a restoration of blood flow following transplantation. To monitor blood flow after MSC transplantation, laser Doppler imaging was performed at days 0, 14, and 28 after surgery. The N-MSC-treated animals had significantly improved blood flow in contrast to the HGPS and culture medium groups ($p < 0.001$) (Figure 7B). Histological examination for the presence of human cells in the affected limbs by human nuclear antigen staining indicated that HGPS-MSC disappear much faster than N-MSC in ischemia limbs. At day 35 after surgery, while some HNA positive cells could be seen in N-MSCs transplanted samples, no positive cells were found in HGPS-MSC treated limbs (Figure 7C).

MSC-mediated, postischemia recovery is attributed to neovasculogenesis due to the secretion of paracrine factors by the transplanted MSCs (Horwitz and Prather, 2009). However, analysis of media conditioned by the various control and HGPS-MSC preparations failed to reveal any differences in the levels of those factors often implicated in neovasculogenesis including VEGF, bFGF, and IL-6 (Figure S5A). We conclude that the poor survival of HGPS-MSCs in ischemic limbs may underlie limb-rescue failure.

MSCs in vivo occupy low oxygen niches and normally exhibit a faster and longer proliferation potential under hypoxic conditions (Dos Santos et al., 2010; Rosova et al., 2008). To determine whether HGPS-MSC loss is due to an acquired sensitivity to ischemia-induced hypoxic conditions, we subjected the cells to hypoxia and substratum deprivation as described earlier. Under normal growth conditions, HGPS-MSC and N-MSCs proliferated at same rate; however, after the hypoxia, only 40% of the HGPS-MSCs survived compared to 80% of the N-MSCs (Figure 6A). TUNEL assay showed that double the number of HGPS-MSCs were apoptotic (Figure 7D). In parallel experiments, HGPS fibroblasts and endothelial cells and their normal controls derived from iPSCs survived, as well as human bone marrow MSCs after hypoxia and substrate deprivation (Figure 6A). These results indicate that HGPS-MSCs are more sensitive to the combination of hypoxia and substrate deprivation. Interestingly, with hypoxia alone (3 days in 2% O_2), very little sensescence was noted in HGPS- and N-MSC populations in contrast to the higher levels in HGPS-VSMCs (Figure 6B).

Antisense morpholinos or shRNAs specifically target and suppress progerin expression (Huang et al., 2005). To demonstrate that the increased sensitivity of the HGPS-MSCs were a consequence of progerin expression, we infected N- or HGPS-MSCs with lentiviral vectors expressing control shRNA and shRNA against progerin. Resistance to hypoxia and substratum deprivation is restored in HGPS-MSCs, when progerin levels were reduced by 65% (Figure 7E and Figure S6), indicating progerin accumulation is responsible for this defect.

Finally, we determined if HGPS-MSCs were susceptible to other forms of stress. Both HGPS-MSC and N-MSCs were cultured in serum-free medium for 10 days. HGPS-MSC numbers declined rapidly; in contrast, N-MSCs and adult bone marrow MSCs survived serum starvation (Figure 7F).

In summary, HGPS fibroblasts, -MSCs, and -VSMCs all display enhanced DNA damage, LAP2 mislocalization, and pronounced nuclear dysmorphology. When exposed to additional stress in vitro and (MSC) in vivo, the viability of VSMCs and MSCs were significantly reduced, with VSMCs showing a particular sensitivity to low oxygen.

DISCUSSION

Mutations in *LMNA* are responsible for more than ten distinct diseases (Mounkes and Stewart, 2004). HGPS is the best known of these laminopathies, with the most common form of HGPS being characterized by the production of the mutant lamin A, progerin. It is widely believed that the pathological effects of progerin are mediated by its disruption of the structural and functional integrity of the nuclear lamina. Autopsies indicated that death is associated with premature atherosclerosis (Olive et al., 2010), which may be accompanied by vascular smooth muscle loss (Stehbens et al., 2001) The limited biopsy data available shows progerin is mainly detected in some keratinocytes, vascular smooth muscle, dermal fibroblast, and endothelial cells (McClintock et al., 2006; Olive et al., 2010). Apart from the patient data, most information on the disease pathophysiology has been inferred from mouse models expressing mutated endogenous *LMNA* alleles or mutated human or mouse *LMNA* transgenes,

(D) Immunostaining of progerin, LMNA, LAP2, and H2AX showed increased number of cells associated with mislocalization of LAP2 and DNA damage in HGPS-VSMCs at p3. The percentage of cells showing abnormal phenotypes is indicated. Scale bar, 20 μm.

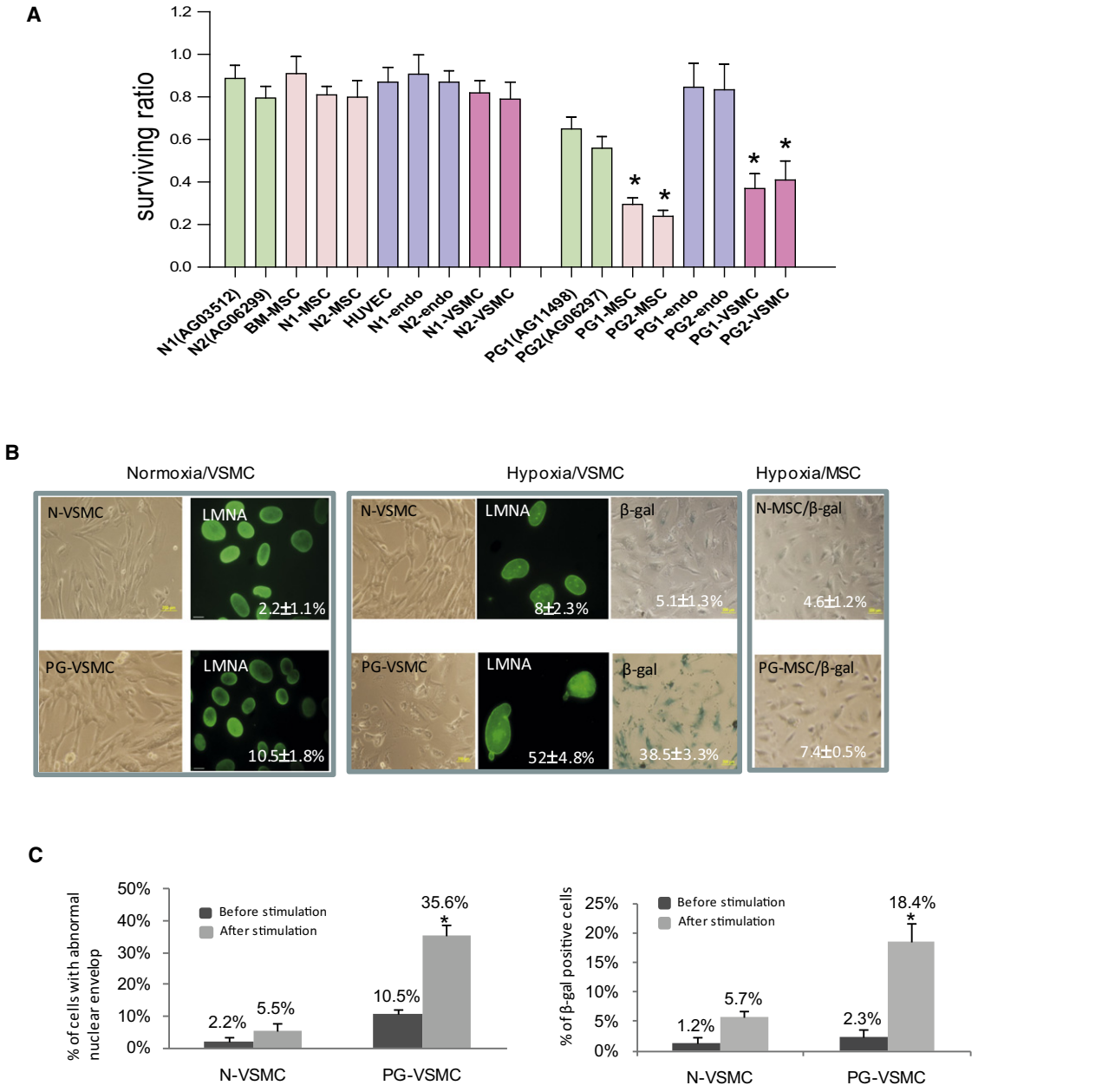

Figure 6. Stress Testing of iPSC-Derived Lineages in Culture

(A) Cell survival rate after treatment with oil immersion and substrate deprivation. Values represent ratio of surviving cells relative to input. Results were obtained from three biological replicates, and experiments were repeated three times. *p < 0.01 compared with controls in left panel, e.g., BM-MSC, N1-iPSC-MSC, N2-iPSC-MSC, HUVEC, N1-iPSC-endo, N2-iPSC-endo, N1-VSMC, and N2-VSMC.

(B) Hypoxia treatment of VSMCs. Cells were incubated in 2% O2 with normal culture medium for 72 hr. Representative phase contrast and immunostaining images show morphology of VSMC and LMNA staining. Cell senescence was detected by β-gal staining. The percentage of cells showing β-gal positive and abnormal nuclei is indicated. Cell senescence is not observed in iPS-MSCs under the same treatment.

(C) Electrical stimulation of VSMCs. Electrical pulses (40V/cm, 1Hz) were applied to VSMCs in culture for a period of 3 days. Increased nuclear dysmorphology by LMNA staining was observed in HGPS-VSMCs (left panel). Accelerated sensescence of HGPS-VSMCs was detected by β-gal staining (right panel). Experiment was repeated, and *p < 0.01 compared with N-iPSC-VSMCs.

studies on cultured patient fibroblasts, or through overexpression of progerin in primary and immortalized human cells.

Although some mouse models with *LMNA* changes show a severe HGPS-like growth retardation and bone disease (Fong et al., 2004; Mounkes et al., 2003; Varga et al., 2006; Yang et al., 2005), no mouse model captures all the human symptoms and, until recently, only one (Varga et al., 2006) displays a cardiovascular phenotype. Hernandez et al. (2010) showed in the murine progeria model (*Lmna*Δ*9*/Δ*9*) that, although the mutant lamin A in this strain has a different internal

deletion to the one found in progerin, it retains a farnesylated tail, resulting in number of characteristic progeric pathologies, including thinning of the VSMC intima. These pathologies were attributed *inter alia* to defective extracellular matrix synthesis. Microarray comparisons of the HGPS and control iPSC-MSCs indicated significant misregulation of transcripts encoding extracellular matrix proteins, as previously reported by Csoka et al. (2004) and Scaffidi and Misteli (2008), although we could not detect the alteration in the named components of the Notch signaling pathway reported by these latter authors (Table S3).

HGPS fibroblasts demonstrate increased nuclear blebbing, mislocalization of the nuclear protein (LAP2), DNA damage, and aberrant chromatin modifications in HGPS cells at late passage as reported for. HGPS fibroblasts or MSCs expressing exogenously added progerin genes (Scaffidi and Misteli, 2008). Apart from fibroblasts, very few other patient-derived cell lineages are available for study. Here, we describe an approach to HGPS modeling that should, in time, allow the production and investigation of multiple HGPS cell lineages with *endogenous* levels of progerin and other lamins.

HGPS fibroblasts were reprogrammed to iPSC by retroviral-mediated integration of the Yamanaka factors OCT4, SOX2, KLF4, and C-MYC (Takahashi et al., 2007). Though the reprogramming efficiency is low compared with normal fibroblasts, the HGPS-iPSCs, once established, were all karyotypically normal and indistinguishable from normal iPSCs and human ESCs in many aspects, including specific marker expression, germ layer formation, epigenetic status, and global transcriptional expression. As expected for pluripotent cell types (Constantinescu et al., 2006), very little progerin, lamin A, or lamin C were detected in the undifferentiated iPSCs. Upon differentiation into fibroblasts, neural progenitors, vascular endothelial cells, VSMCs, and MSCs, the *LMNA* gene is transcriptionally activated and progerin levels increase. We observed the highest levels of progerin (and the highest levels of DNA damage, LAP2 mislocalization, and nuclear dysmorphology) in HGPS-iPSC derived MSCs, VSMCs, and fibroblasts, slightly less in endothelial cells and very little in neural progenitors. These differences are likely to reflect inherent variation in the production and/or turnover of progerin in the different cell types and the relationship between progerin level and damage may, if extended over many more cell types, track the more affected tissues in HGPS patients.

Progerin did not affect either the efficiency of differentiation of iPSCs into MSCs, VSMCs, endothelial cells, and neural progenitors, or the proliferation rate of these cell types. It did not functionally interfere with lattice formation or LDL uptake in the endothelial cells, or with neuron formation from the neural progenitors. We also noticed a new and completely unexpected phenotype in many of the HGPS-VSMCs: the appearance of heterogeneously sized, calponin 1-staining inclusion bodies in the cytoplasm (Figure 5). Calponin1 is an actin-binding protein involved in the regulation of smooth muscle contraction, possibly by inhibiting actin-activated myosin ATP-ase activity (Takahashi and Yamamura, 2003). We speculate that its sequestration into aggregates could affect the contractile properties of the VSMC in situ. HGPS-VSMCs were also very sensitive to 2% hypoxia and to the combination of hypoxia and substratum deprivation. Furthermore, when HGPS-VSMCs were subjected to repeated pulses of electrical stimulation, they rapidly senesced; in the context of the vascular system, electrical stimulation has been used to enhance angiogenesis (Zhao et al., 2004), to improve engineered myocardium (Radisic et al., 2004) and, in this study, to act as a surrogate means of mimicking the hemodynamic shear stress normally endured by VSMCs in vivo. This pronounced sensitivity of the HGPS-VSMCs to various imposed insults, as well as the possible perturbation of contractile properties due to calponin sequestration, may explain why this lineage features prominently in the pathology of progeria.

HGPS and control iPSC-MSCs were differentiated into bone, cartilage, and fat. We could not determine whether the efficiency of differentiation into the various lineages was affected by the presence of progerin, unlike Scaffidi and Misteli (2008), who reported that adipogenesis was impaired while osteogenesis was stimulated by progerin. We did not note any impact of progerin on adipogenesis, although osteogenenic differentiation varied, but not in a progerin-specific manner (Figure 4E). However, we believe the two sets of experiments are not comparable since Scaffidi and Misteli (2008) obtained their results by manipulation of a single MSC genotype, while each iPSC-MSC population used in our study represented a different genotype, and it is known that human MSC differentiation is influenced by donor genotype (Leskela et al., 2006). We, therefore, elected to functionally test iPSC-MSCs in vivo. Using a hind limb ligation mouse model that measures limb survival and the restoration of blood flow after cell transplantation, we found that HGPS-MSCs were only slightly better than the vehicle in saving the ischemic limb, in contrast to the successful rescue mediated by control iPSC-MSCs or adult bone marrow MSCs. Microarray comparisons between HGPS-MSCs and control MSCs showed no obvious change in angiogenic factors such as VEGF, bFGF, and Il-6, results confirmed by direct analysis of conditioned media (Figure S5A). The histology of salvaged limbs showed no long-term integration of any of the transplanted populations and that HGPS-MSCs were cleared more rapidly than control cells. We speculate that the HGPS-MSCs are cleared before they can exert any trophic effect on the neighboring tissues. This rapid clearance could reflect a greater sensitivity of HGPS-MSCs to the ischemic conditions or to stress in general. Accordingly, we stressed the cells in two ways: first, we studied their reaction to serum starvation and found the HGPS-MSC numbers rapidly declined (Figure 7F) and second, we deprived cells of oxygen and substratum (Weil et al., 2009). Compared to the control cells, survival of the HGPS-MSCs was significantly reduced, an effect that was mostly reversed by a 65% decrease in cellular progerin as a result of specific shRNA knockdown. We, therefore, conclude that HGPS-MSC are particularly sensitive to this type of hypoxic condition and believe that this is a significant finding because MSCs normally reside in low O_2 niches within the body (Rosova et al., 2008). We do not yet have a molecular explanation for this difference; transcript levels of one obvious candidate-Hypoxia-Inducing Factor 1 were similar in control and HGPS-MSCs, at least under normoxic conditions (Figure S5B). In vivo, the exact roles of MSCs are unclear, although they may be a source of VSMCs and pericytes, but it is generally agreed that they are important for tissue maintenance and repair. One hypothesis, for the underlying pathology of HGPS, is that progerin inhibits cell replacement in the cardiovascular system, hair follicles, fat, and cartilage due to premature exhaustion of

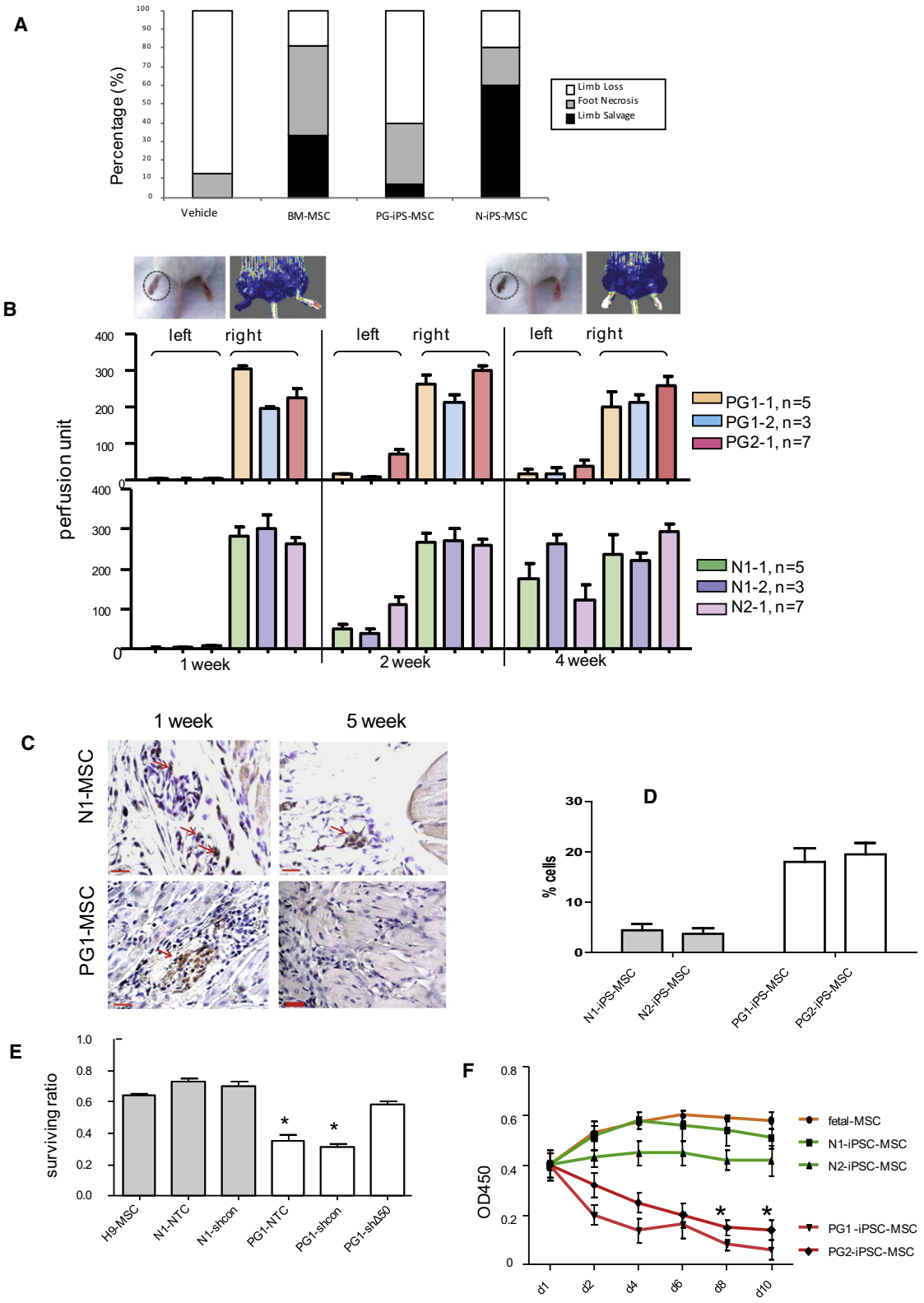

Figure 7. Rescue of Ischemic Murine Hind Limb Using Transplanted iPSC-Derived MSCs

(A) Transplantation of HGPS-iPSC-MSCs failed to attenuate hind-limb ischemia. At day 28 after transplantation of bone marrow or iPSC-derived MSCs, the physiological status of ischemic limbs were rated for limb salvage, foot necrosis, and limb loss. The BM-MSC ($p = 0.0058$) and N-iPSC-MSC ($p = 0.0092$), but not HGPS-iPSC-MSC ($p = 0.2779$), showed significant rescue of ischemia. Student's t test (two tail) comparison with vehicle is used for analysis ($n = 8$ for vehicle, $n = 15$ per group).

stem cell pools (Halaschek-Wiener and Brooks-Wilson, 2007), perhaps by inhibiting Wnt signaling (Hernandez et al., 2010; Meshorer and Gruenbaum, 2008). Our findings lead us to propose a refinement to their model and suggest that in addition to the "exhaustion" caused by the need to replace lost mesenchymal tissue, the MSC pool is also depopulated due to increased hypoxia sensitivity caused by progerin. Given the historical (Horwitz and Prather, 2009) and current clinical trials (http://clinicaltrials.gov/ct2/show/NCT01061099) using allogeneic MSCs for another congenital disease, osteogenesis imperfecta, our data suggest MSCs may be of therapeutic use for HGPS patients.

To our knowledge, this is the first report of an iPSC-based disease model of HGPS. It complements existing approaches using animal and cell models, and the achievement of tissue-specific expression of a disease-associated gene at endogenous levels must be considered an attractive feature. This general approach is still young and faces numerous challenges, particularly regarding the appropriateness of using embryonic starting material to model neonatal and adult onset diseases (Colman and Dreesen, 2009; Saha and Jaenisch, 2009). We are encouraged by the demonstration that the HGPS-iPSCs can yield distinctive phenotypes, e.g., VSMCs and MSCs, that lead to specific predictions that could be tested with suitable animal and cellular models and/or patient material.

EXPERIMENTAL PROCEDURES

Cell Culture

HGPS patient fibroblast cells, adult human bone marrow MSCs, human umbilical cord endothelial cells (HUVECs), and the human neural stem cell line (ReNcells) were purchased from Coriell cell repositories (http://ccr.coriell.org/), Lonza, and Millipore, respectively. Fetal bone marrow MSC was obtained from S.K. Lim (Institute of Medical Biology, Singapore). All cell cultures were maintained at 37°C with 5% CO_2. Human embryonic stem cell lines (hESCs) HES3, H9, and induced pluripotent stem cells (iPSCs) were cultured on irradiated mouse embryonic fibroblasts (MEFs) with Knockout DMEM medium supplemented with 20% knockout serum replacement, nonessential amino acid, 2-mercaptoethanol, penicillin/streptomycin, GlutaMax, and bFGF. Cells were passaged with collagenase IV (all GIBCO). The hypoxia and substrate deprivation assay was performed according to Weil et al. (2009). Cells were harvested using 0.25% Trypsin-EDTA and pelleted by centrifugation. 3×10^5 cells were exposed to 2–4 hr of hypoxia via mineral oil immersion followed by reoxygenation in normal conditions for 24 hr. Surviving cells were counted using Trypan blue stain.

Retroviral Production and iPS Generation

The pMX-based retroviral vector encoding the human cDNAs of *KLF4*, *SOX2*, *OCT4*, and *C-MYC* were obtained from Addgene. Retrovirus was produced as described (Dimos et al., 2008). Briefly, pMXs plasmids were cotransfected with packaging plasmid gag-pol and VSV-G into 293T packaging cells (ATCC) using SuperFect (QIAGEN). Viral supernatant fractions were harvested after 60 hr, filtered through a 0.45 μm low protein binding cellulose acetate filter, and concentrated by centrifugation. To produce patient-specific iPSCs, two rounds of viral transduction of 100,000 fibroblast cells were performed. After 4 days, cells were transferred onto MEFs in human ESC medium containing 0.5 mM valproic acid (VPA, Sigma). iPSC colonies were manually picked after 2 to 3 weeks.

Differentiation of iPSCs into Fibroblast-like Cells

The human ESCs and iPSCs were harvested using collagenase IV and embryoid bodies (EBs) were formed and transferred to gelatin-coated plates in differentiation medium as described (Xu et al., 2004). The cells were subsequently passaged with medium containing 90% DMEM (Invitrogen), 10% heat-inactivated FBS (Hyclone), 2mM L-glutamine, and 1% nonessential amino acids. Cells were further purified with Thy1 antibody by FACS sorter. The identity of the established fibroblast-like cells was confirmed with immunostaining by antibody against human fibroblast/epithelial cells (Novus Biologicals, D7-FIB) and prolyl4-hydroxylase, an enzyme required for collagen synthesis.

Differentiation of VSMCs from MSCs

VSMCs were differentiated from iPSC-MSCs by culturing in EGM-2 medium (Lonza) with sphingosylphosphorylcholine (SPC, 5 μM) and TGFβ1 (2 ng/ml) for 3 weeks. The identity of VSMCs was verified by specific marker expression of smooth muscle actin, smooth muscle myosin heavy chain and calponin by RT-PCR and immune-staining (all DAKO 1:100). Contraction of VSMCs was induced by carbachol at 1×10^{-5} M for 1 hr. Electrical stimulation was applied to VSMCs using C-pace/C-dish cell culture stimulation system (IonOptix, MA) at 40V, 1 Hz with pulse duration of 2 ms.

Knockdown of Progerin in HGPS-iPS-MSCs by Lentiviral Infection

ShRNA-specific knockdown of lamin AΔ50 (progerin), but not lamin A or C, was designed according to Huang et al. (2005). Oligonucleotides encoding the hairpin shRNA (shΔ50) targeting the sequence (5′-GGC TCA GGA GCC CAG AGC CCC-3′) were cloned into the lentiviral vector plko.3G (Addgene). A shRNA that does not target any mammalian gene (5′-TTC TCC GAA CGT GTC ACGT-3′) was used as control (shcon). For lentivirus production, lentiviral vectors were cotransfected with packaging vectors into 293FT cells, and the

(B) The dynamic change of blood flow after MSC transplantation. Hind limb ischemia was created by ligation of the left hind limb femoral artery. The right hind limb was used as control for blood flow measurement using laser Doppler flow imaging. Representative Doppler photo shows no blood flow upon ligation (left panel) and restoration of blood flow 28 days after MSC transplantation (right panel). Restoration of blood flow in the HGPS-iPSC-MSC transplanted group is significantly lower than N-iPSC-MSC group at 4 weeks. ($p < 0.001$, $n = 15$ per group). Three iPSC clones (PG1-iPSC-1, PG1-iPSC-2, and PG2-iPSC-1) from two different patient fibroblasts were used to derive the MSCs used for transplantation.

(C) Immunostaining of human nuclear antigen (HNA) in ischemic limb tissues. Mice tissues were paraformaldehyde fixed, paraffin embedded, and sectioned for immunostaining using antibody against HNA. Human cells stained brown (red arrow) were not found anywhere in HGPS-iPSC-MSC transplanted tissues after 5 weeks. Scale bar, 200 μm.

(D) Percentage of cell death after hypoxia and substrate deprivation treatment. Apoptotic cells were label by TUNEL (TdT-mediated dUTP nick end labeling) and analyzed by FACS. Results were each obtained from three biological replicates. N1-iPSC-MSC/N2-iPSC-MSC shows significantly more resistant than PG1-iPSC-MSC/PG2-iPSC-MSC ($p < 0.01$).

(E) Knocking down progerin in HGPS-iPSC-MSC improves survival in hypoxia and substrate deprivation assay. Cells were transfected with lentivirus-containing shRNAs before being challenged. Values represent ratio of surviving cells relative to input. Results were obtained from three biological replicates, and experiments were repeated two times. *$p < 0.01$ compared with H9-derived MSC, N1-NTC (N1-iPSC-MSC Non-Transduction Control), N1-shcon (N1-iPSC-MSC expressing control shRNA), and PG1-shΔ50 (HGPS-iPSC-MSC expressing shRNA against progerin).

(F) Cell proliferation in serum-free medium. HGPS or control iPSC-derived MSCs or bone marrow MSCs were seeded at a density of 4×10^4 per well in triplicate for each line and cell survival was measured using a WST-1 kit (Roche) according to the manufacturer's protocol. Value represents mean ± SD *$p < 0.01$ compared with three normal control groups.

See also Figure S4 for representative images of fibrosis in hind limbs of ischemic mice, Figure S5 for characterization of hypoxia related factors, and Figure S6 for progerin shRNA and lamin expression.

supernatant was harvested and concentrated by ultracentrifugation for 1.5 hr at 25,000 r.p.m. in a Beckman SW28 rotor. Titers were determined by infecting NIH/3T3 cells with a serial dilution of the concentrated virus. For a typical preparation, the titer was approximately 1–5 × 10^7/ml. 2 × 10^5 cells were incubated in suspension with 1 × 10^6 particles and 8 μg/ml polybrene for 3 hr in a 37°C incubator. The cells were then replated and cultured as described. GFP-positive cells were sorted after 4 days of culture.

Limb Ischemia and Transplantation Studies

SCID mice were anesthetized with xylazine (20 mg/kg) and ketamine (100 mg/kg), and critical limb ischemia was induced as described previously (Lian et al., 2010). The femoral artery and its branches were ligated through a skin incision with 5-0 silk (Ethicon, Somerville, NJ). The external iliac artery and all of the above arteries were then ligated. The femoral artery was excised from its proximal origin as a branch of the external iliac artery to the distal point where it bifurcates into the saphenous and poplite arteries. After arterial ligation, SCID mice were immediately assigned to the following experimental groups: (1) N-iPS-MSC group: the mice were injected with MSCs derived from normal control iPSCs (3.0 × 10^6 cells per mouse in 200 μL) intramuscularly at four sites of the gracilis muscle in the medial thigh with 29-gauge tuberculin syringes; (2) PG- iPS-MSC: the mice were injected as above with MSCs derived from HGPS patient iPSCs. Fetal bone marrow (BM)-MSC and culture medium (vehicle) were used as controls. To exclude the possibility of bacterial infection following surgery being responsible for poor recovery, specimens of the ischemic muscle were cultured on day 7 after surgery and no bacterial growth was detected in each group. All animal experiments were approved by Committee on the Use of Live Animals in Teaching and Research (CULTAR) at the University of Hong Kong.

Laser Doppler Imaging Analysis

Laser Doppler imaging analysis was performed as described previously (Lian et al., 2010). A laser Doppler perfusion imager (Moor Instruments, Devon, United Kingdom) was used for serial scanning of surface blood flow of hindlimbs on days 0, 7, 14, and 28 after treatment. The digital color-coded images were analyzed to quantify the blood flow in the region from the knee joint to the toe, and mean values of perfusion were calculated.

ACCESSION NUMBERS

Microarray data has been deposited in the GEO database (GSE26093).

SUPPLEMENTAL INFORMATION

Supplemental Information includes six figures, three tables, and Supplemental Experimental Procedures and can be found with this article online at doi:10.1016/j.stem.2010.12.002.

ACKNOWLEDGMENTS

We thank the Singapore Biomedical Research Council and the Singapore Agency for Science, Technology and Research (A*STAR) for funding this work. The animal work was supported by Hong Kong Research Grant Council (HKU 8/CRF/09). We also thank M. Costa for helpful advice.

Received: June 3, 2010
Revised: October 18, 2010
Accepted: December 6, 2010
Published online: December 23, 2010

REFERENCES

Ackerman, J., and Gilbert-Barness, E. (2002). Hutchinson-Gilford progeria syndrome: a pathologic study. Pediatr. Pathol. Mol. Med. *21*, 1–13.

Agarwal, S., Loh, Y.H., McLoughlin, E.M., Huang, J., Park, I.H., Miller, J.D., Huo, H., Okuka, M., Dos Reis, R.M., Loewer, S., et al. (2010). Telomere elongation in induced pluripotent stem cells from dyskeratosis congenita patients. Nature *464*, 292–296.

Bridger, J.M., and Kill, I.R. (2004). Aging of Hutchinson-Gilford progeria syndrome fibroblasts is characterised by hyperproliferation and increased apoptosis. Exp. Gerontol. *39*, 717–724.

Burke, B., and Stewart, C.L. (2006). The laminopathies: the functional architecture of the nucleus and its contribution to disease. Annu. Rev. Genomics Hum. Genet. *7*, 369–405.

Cao, K., Capell, B.C., Erdos, M.R., Djabali, K., and Collins, F.S. (2007). A lamin A protein isoform overexpressed in Hutchinson-Gilford progeria syndrome interferes with mitosis in progeria and normal cells. Proc. Natl. Acad. Sci. USA *104*, 4949–4954.

Capell, B.C., and Collins, F.S. (2006). Human laminopathies: nuclei gone genetically awry. Nat. Rev. Genet. *7*, 940–952.

Colman, A., and Dreesen, O. (2009). Pluripotent stem cells and disease modelling. Cell Stem Cell *5*, 244–247.

Constantinescu, D., Gray, H.L., Sammak, P.J., Schatten, G.P., and Csoka, A.B. (2006). Lamin A/C expression is a marker of mouse and human embryonic stem cell differentiation. Stem Cells *24*, 177–185.

Csoka, A.B., English, S.B., Simkevich, C.P., Ginzinger, D.G., Butte, A.J., Schatten, G.P., Rothman, F.G., and Sedivy, J.M. (2004). Genome-scale expression profiling of Hutchinson-Gilford progeria syndrome reveals widespread transcriptional misregulation leading to mesodermal/mesenchymal defects and accelerated atherosclerosis. Aging Cell *3*, 235–243.

De Sandre-Giovannoli, A., Bernard, R., Cau, P., Navarro, C., Amiel, J., Boccaccio, I., Lyonnet, S., Stewart, C.L., Munnich, A., Le Merrer, M., et al. (2003). Lamin a truncation in Hutchinson-Gilford progeria. Science *300*, 2055.

Dimos, J.T., Rodolfa, K.T., Niakan, K.K., Weisenthal, L.M., Mitsumoto, H., Chung, W., Croft, G.F., Saphier, G., Leibel, R., Goland, R., et al. (2008). Induced pluripotent stem cells generated from patients with ALS can be differentiated into motor neurons. Science *321*, 1218–1221.

Dos Santos, F., Andrade, P.Z., Boura, J.S., Abecasis, M.M., da Silva, C.L., and Cabral, J.M. (2010). Ex vivo expansion of human mesenchymal stem cells: a more effective cell proliferation kinetics and metabolism under hypoxia. J. Cell. Physiol. *223*, 27–35.

Ebert, A.D., Yu, J., Rose, F.F., Jr., Mattis, V.B., Lorson, C.L., Thomson, J.A., and Svendsen, C.N. (2009). Induced pluripotent stem cells from a spinal muscular atrophy patient. Nature *457*, 277–280.

Fong, L.G., Ng, J.K., Meta, M., Coté, N., Yang, S.H., Stewart, C.L., Sullivan, T., Burghardt, A., Majumdar, S., Reue, K., et al. (2004). Heterozygosity for Lmna deficiency eliminates the progeria-like phenotypes in Zmpste24-deficient mice. Proc. Natl. Acad. Sci. USA. *101*, 18111–18116.

Goldman, R.D., Shumaker, D.K., Erdos, M.R., Eriksson, M., Goldman, A.E., Gordon, L.B., Gruenbaum, Y., Khuon, S., Mendez, M., Varga, R., et al. (2004). Accumulation of mutant lamin A causes progressive changes in nuclear architecture in Hutchinson-Gilford progeria syndrome. Proc. Natl. Acad. Sci. USA *101*, 8963–8968.

Gordon, L.B., McCarten, K.M., Giobbie-Hurder, A., Machan, J.T., Campbell, S.E., Berns, S.D., and Kieran, M.W. (2007). Disease progression in Hutchinson-Gilford progeria syndrome: impact on growth and development. Pediatrics *120*, 824–833.

Halaschek-Wiener, J., and Brooks-Wilson, A. (2007). Progeria of stem cells: stem cell exhaustion in Hutchinson-Gilford progeria syndrome. J. Gerontol. A Biol. Sci. Med. Sci. *62*, 3–8.

Hanna, J., Saha, K., Pando, B., van Zon, J., Lengner, C.J., Creyghton, M.P., van Oudenaarden, A., and Jaenisch, R. (2009). Direct cell reprogramming is a stochastic process amenable to acceleration. Nature *462*, 595–601.

Hennekam, R.C. (2006). Hutchinson-Gilford progeria syndrome: review of the phenotype. Am. J. Med. Genet. *140*, 2603–2624.

Hernandez, L., Roux, K.J., Wong, E.S., Mounkes, L.C., Mutalif, R., Navasankari, R., Rai, B., Cool, S., Jeong, J.W., Wang, H., et al. (2010). Functional coupling between the extracellular matrix and nuclear lamina by Wnt signaling in progeria. Dev. Cell *19*, 413–425.

Horwitz, E.M., and Prather, W.R. (2009). Cytokines as the major mechanism of mesenchymal stem cell clinical activity: expanding the spectrum of cell therapy. Isr. Med. Assoc. J. *11*, 209–211.

Huang, S., Chen, L., Libina, N., Janes, J., Martin, G., Campisi, J., and Oshima, J. (2005). Correction of cellular phenotypes of Hutchinson-Gilford Progeria cells by RNA interference. Hum. Genet. *118*, 444–450.

Jeon, E.S., Moon, H.J., Lee, M.J., Song, H.Y., Kim, Y.M., Bae, Y.C., Jung, J.S., and Kim, J.H. (2006). Sphingosylphosphorylcholine induces differentiation of human mesenchymal stem cells into smooth-muscle-like cells through a TGF-beta-dependent mechanism. J. Cell Sci. *119*, 4994–5005.

Lee, G., Papapetrou, E.P., Kim, H., Chambers, S.M., Tomishima, M.J., Fasano, C.A., Ganat, Y.M., Menon, J., Shimizu, F., Viale, A., et al. (2009). Modelling pathogenesis and treatment of familial dysautonomia using patient-specific iPSCs. Nature *461*, 402–406.

Leskela, H.V., Olkku, A., Lehtonen, S., Mahonen, A., Koivunen, J., Turpeinen, M., Uusitalo, J., Pelkonen, O., Kangas, L., Selander, K., et al. (2006). Estrogen receptor alpha genotype confers interindividual variability of response to estrogen and testosterone in mesenchymal-stem-cell-derived osteoblasts. Bone *39*, 1026–1034.

Li, Q., Yao, D., Ma, J., Zhu, J., Xu, X., Ren, Y., Ding, X., and Mao, X. (2009). Transplantation of MSCs in combination with Netrin-1 improves neoangiogenesis in a rat model of hind limb ischemia. J. Surg. Res. Published online September 23, 2009. 10.1016/j.jss.2009.08.031.

Lian, Q., Zhang, Y., Zhang, J., Zhang, H.K., Wu, X., Zhang, Y., Lam, F.F., Kang, S., Xia, J.C., Lai, W.H., et al. (2010). Functional mesenchymal stem cells derived from human induced pluripotent stem cells attenuate limb ischemia in mice. Circulation *121*, 1113–1123.

McClintock, D., Gordon, L.B., and Djabali, K. (2006). Hutchinson-Gilford progeria mutant lamin A primarily targets human vascular cells as detected by an anti-Lamin A G608G antibody. Proc. Natl. Acad. Sci. USA *103*, 2154–2159.

McClintock, D., Ratner, D., Lokuge, M., Owens, D.M., Gordon, L.B., Collins, F.S., and Djabali, K. (2007). The mutant form of lamin A that causes Hutchinson-Gilford progeria is a biomarker of cellular aging in human skin. PLoS ONE *2*, e1269.

Merideth, M.A., Gordon, L.B., Clauss, S., Sachdev, V., Smith, A.C., Perry, M.B., Brewer, C.C., Zalewski, C., Kim, H.J., Solomon, B., et al. (2008). Phenotype and course of Hutchinson-Gilford progeria syndrome. N. Engl. J. Med. *358*, 592–604.

Meshorer, E., and Gruenbaum, Y. (2008). Gone with the Wnt/Notch: stem cells in laminopathies, progeria, and aging. J. Cell Biol. *181*, 9–13.

Mounkes, L.C., and Stewart, C.L. (2004). Aging and nuclear organization: lamins and progeria. Curr. Opin. Cell Biol. *16*, 322–327.

Mounkes, L.C., Kozlov, S., Hernandez, L., Sullivan, T., and Stewart, C.L. (2003). A progeroid syndrome in mice is caused by defects in A-type lamins. Nature *423*, 298–301.

Musich, P.R., and Zou, Z. (2009). Genomic instability and DNA damage responses in progeria arising from defective maturation of prelamin A. Aging *1*, 28–37.

Olive, M., Harten, I., Mitchell, R., Beers, J., Djabali, K., Cao, K., Erdos, M.R., Blair, C., Funke, B., Smoot, L., et al. (2010). Cardiovascular Pathology in Hutchinson-Gilford Progeria: Correlation With the Vascular Pathology of Aging. Arterioscler. Thromb. Vasc. Biol. *30*, 2301–2309.

Radisic, M., Park, H., Shing, H., Consi, T., Schoen, F.J., Langer, R., Freed, L.E., and Vunjak-Novakovic, G. (2004). Functional assembly of engineered myocardium by electrical stimulation of cardiac myocytes cultured on scaffolds. Proc. Natl. Acad. Sci. USA *101*, 18129–18134.

Rosova, I., Dao, M., Capoccia, B., Link, D., and Nolta, J.A. (2008). Hypoxic preconditioning results in increased motility and improved therapeutic potential of human mesenchymal stem cells. Stem Cells *26*, 2173–2182.

Sagelius, H., Rosengardten, Y., Hanif, M., Erdos, M.R., Rozell, B., Collins, F.S., and Eriksson, M. (2008). Targeted transgenic expression of the mutation causing Hutchinson-Gilford progeria syndrome leads to proliferative and degenerative epidermal disease. J. Cell Sci. *121*, 969–978.

Saha, K., and Jaenisch, R. (2009). Technical challenges in using human induced pluripotent stem cells to model disease. Cell Stem Cell *5*, 584–595.

Scaffidi, P., and Misteli, T. (2006). Lamin A-dependent nuclear defects in human aging. Science *312*, 1059–1063.

Scaffidi, P., and Misteli, T. (2008). Lamin A-dependent misregulation of adult stem cells associated with accelerated ageing. Nat. Cell Biol. *10*, 452–459.

Stehbens, W.E., Delahunt, B., Shozawa, T., and Gilbert-Barness, E. (2001). Smooth muscle cell depletion and collagen types in progeric arteries. Cardiovasc. Pathol. *10*, 133–136.

Takahashi, K., and Yamamura, H. (2003). Studies and perspectives of calponin in smooth muscleregulation and cancer gene therapy. Adv. Biophys. *3*, 91–111.

Takahashi, K., Tanabe, K., Ohnuki, M., Narita, M., Ichisaka, T., Tomoda, K., and Yamanaka, S. (2007). Induction of pluripotent stem cells from adult human fibroblasts by defined factors. Cell *131*, 861–872.

Varga, R., Eriksson, M., Erdos, M.R., Olive, M., Harten, I., Kolodgie, F., Capell, B.C., Cheng, J., Faddah, D., Perkins, S., et al. (2006). Progressive vascular smooth muscle cell defects in a mouse model of Hutchinson-Gilford progeria syndrome. Proc. Natl. Acad. Sci. USA *103*, 3250–3255.

Verstraeten, V.L., Ji, J.Y., Cummings, K.S., Lee, R.T., and Lammerding, J. (2008). Increased mechanosensitivity and nuclear stiffness in Hutchinson-Gilford progeria cells: effects of farnesyltransferase inhibitors. Aging Cell *7*, 383–393.

Weil, B.R., Markel, T.A., Herrmann, J.L., Abarbanell, A.M., and Meldrum, D.R. (2009). Mesenchymal stem cells enhance the viability and proliferation of human fetal intestinal epithelial cells following hypoxic injury via paracrine mechanisms. Surgery *146*, 190–197.

Xu, C., Jiang, J., Sottile, V., McWhir, J., Lebowski, J., and Carpenter, M.K. (2004). Immortalized fibroblast-like cells derived from human embryonic stem cells support undifferentiated cell growth. Stem Cells *22*, 972–980.

Yang, S.H., Bergo, M.O., Toth, J.I., Qiao, X., Hu, Y., Sandoval, S., Meta, M., Bendale, P., Gelb, M.H., Young, S.G., et al. (2005). Blocking protein farnesyltransferase improves nuclear blebbing in mouse fibroblasts with a targeted Hutchinson-Gilford progeria syndrome mutation. Proc. Natl. Acad. Sci. USA *102*, 10291–10296.

Yang, S.H., Andres, D.A., Spielmann, H.P., Young, S.G., and Fong, L.G. (2008). Progerin elicits disease phenotypes of progeria in mice whether or not it is farnesylated. J. Clin. Invest. *118*, 3291–3300.

Zhao, M., Bai, H., Wang, E., Forrester, J.V., and McCaig, C.D. (2004). Electrical stimulation directly induces pre-angiogenic responses in vascular endothelial cells by signaling through VEGF receptors. J. Cell Sci. *117*, 397–405.